Chaos, Solitons and Fractals 211 (2026) 118804

Contents lists available at ScienceDirect

Chaos, Solitons and Fractals

journal homepage: www.elsevier.com/locate/chaos

Intermittency of fractional optical turbulence

Saad Alhadlaq [a,*], Sergey A. Ponomarenko [a,b]

[a] Department of Electrical and Computer Engineering, Dalhousie University, Halifax, B3J 2X4, Nova Scotia, Canada
[b] Department of Physics and Atmospheric Science, Dalhousie University, Halifax, B3H 4R2, Nova Scotia, Canada

ARTICLE INFO

Keywords:
Fractional NLSE
Lévy index
Fractional optical turbulence
Intermittency

ABSTRACT

We introduce the concept of fractional wave turbulence governed by the fractional nonlinear Schrödinger equation with statistically stationary initial conditions. We explore non-Gaussian statistics and the intermittency of fractional optical turbulence in a stationary regime as a function of the Lévy index. We employ the high-pass filtered kurtosis of a random field as a statistical metric to quantify the strength of intermittency and to highlight the subtle nature of the Lévy index. We discover a non-monotonic dependence of the intermittency strength on the Lévy index of fractional turbulence and identify a range of Lévy indices where intermittent effects are especially pronounced.

1. Introduction

In the context of classical turbulence, intermittency manifests itself as non-uniform, sporadic turbulent bursts at fine scales in space or time [1–3]. The pronounced fine-scale deviations of statistical averages from the predictions of the central limit theorem (Gaussian statistics) are the hallmark of intermittency. The intermittency of classical turbulence was attributed by Kraichnan to the tremendous amplification of minute fluctuations of the dissipation rate of turbulent flows at small scales [4]. A detailed mathematical theory of dissipation-range intermittency was developed in connection with a wide class of nonlinear dynamical systems [5,6]. Remarkably, intermittency can also arise in the stochastic evolution of conservative nonlinear wave systems [7]. The term integrable turbulence was coined to describe the turbulent behavior of weakly dispersive nonlinear waves governed by the (integrable) nonlinear Schrödinger equation with statistically stationary initial conditions [8–10]. The study of integrable turbulence has two major advantages. First, the (integrable) nonlinear Schrödinger equation (NLSE) is effectively one-dimensional, $(1+1)$D to be exact. The lower dimensionality of integrable wave turbulence relative to that of classical turbulence (which is $(3+1)$D) is conducive to an accurate quantitative examination of multiple aspects of wave turbulence. Second, integrable turbulence can be easily realized in optical fibers [11], facilitating its experimental exploration [12].

At the same time, there has been growing interest in wave systems with fractional dispersion. The researchers' curiosity was originally piqued by a rather academic study of the evolution of quantum particles whose phase space trajectories correspond to Lévy flights instead of the usual Brownian motion [13]. These Lévy flights can be quantitatively understood within the framework of the fractional linear Schrödinger equation. The mathematical analogy between the (linear) Schrödinger equation of quantum mechanics and the paraxial wave equation of optics prompted much research into fractional paraxial optics in the context of beams in free space or optical pulses in fibers experiencing either fractional diffraction or fractional dispersion [14,15]. This research has been naturally extended to nonlinear waves in systems with fractional dispersion/diffraction, governed by the fractional nonlinear Schrödinger equation (FNLSE), which has led to the exploration of modulation instability and solitons in such systems [16–22].

However, to our knowledge, studies of nonlinear wave systems obeying the FNLSE have so far been almost exclusively concerned with coherent waves. Here, we introduce the concept of fractional wave turbulence, which is triggered by statistically stationary input noise in wave systems governed by the FNLSE. The FNLSE regime can be realized by engineering fractional dispersion of

* Corresponding author.
E-mail address: s.alhadlaq@dal.ca (S. Alhadlaq).

https://doi.org/10.1016/j.chaos.2026.118804
Received 28 April 2026; Received in revised form 5 July 2026; Accepted 6 July 2026
Available online 19 July 2026

optical waves with the aid of a programmable spatial light modulator (SLM) [23,24]. This opens up the opportunity to implement *fractional optical turbulence (FOT)* in the laboratory. We note in passing that a recently studied scenario of rogue wave generation at the nonlinear stage of modulation instability of a plane wave driven by weak noise [25] does not constitute FOT because the emerging statistics of random waves are not stationary. This is essentially a complementary regime of non-stationary soliton turbulence seeded by modulation instability [25].

In this work, we study the statistics of fractional optical turbulence numerically. The rationale for these studies is twofold. First, fractional wave systems with the Lévy index $\alpha < 2$ feature weaker dispersion/diffraction than do conventional ones, thus allowing insight into a strongly nonlinear regime of wave turbulence even in weakly nonlinear media. Second, fractional wave systems provide fertile ground for extreme events, which are bound to occur more frequently in the strongly nonlinear regime. This triggers a fundamental question: Is FOT intermittent? If so, how is intermittency affected by the magnitude of the Lévy index, a control parameter that is not available for conventional optical turbulence?

Here, we reveal non-Gaussian statistics and intermittency of fractional optical turbulence in a stationary regime as a function of the Lévy index. We employ the high-pass filtered kurtosis of a random field as a statistical metric to quantify the strength of intermittency. Most intriguingly, we unveil a non-monotonic dependence of the intermittency strength on the Lévy index of fractional turbulence and identify a range of Lévy indices where intermittent effects are especially pronounced.

This work is organized as follows. In Section 2, we present our statistical model of FOT, followed by the discussion of our numerical results in Section 3. We summarize our findings in Section 4.

2. Theoretical model

Fractional optical turbulence is governed by the FNLSE of the form

$$i\partial_{z'}\psi + \frac{1}{2}D\left(-\partial^2_{t't'}\right)^{\alpha/2}\psi + \gamma|\psi|^2\psi = 0, \tag{1}$$

where D and γ are effective dispersion and nonlinearity coefficients. The Lévy index α can take on any nonnegative real values; the parameter range $1 \le \alpha \le 2$ corresponds to Lévy flights where the range $\alpha > 2$ gives rise to a generalized FNLSE describing higher order fractional dispersion. The fractional derivative in Eq. (1) should be understood as a Riesz derivative [15,22], defined as

$$(-\partial^2_{t't'})^{\alpha/2}\psi = \int_{-\infty}^{\infty} d\omega\,|\omega|^{\alpha}\tilde{\psi}(\omega)e^{-i\omega t'} = \int_{-\infty}^{\infty} d\omega\,|\omega|^{\alpha}\int_{-\infty}^{\infty}\frac{ds}{2\pi}\,\psi(s)e^{-i\omega(t'-s)}. \tag{2}$$

In light of a possible experimental realization in optical fibers, we work with optical waves whose spatial degrees of freedom are confined by the fiber, justifying a reduction in dimensionality to $(1+1)$D.

Introducing a characteristic time scale σ_t and the corresponding dispersion length $L_\alpha = \sigma_t^\alpha/|D|$, we can rewrite the FNLSE in dimensionless variables as:

$$i\partial_z\Psi - \tfrac{1}{2}(-\partial^2_{tt})^{\alpha/2}\Psi + |\Psi|^2\Psi = 0, \tag{3}$$

where $t = t'/\sigma_t$, $z = z'/L_\alpha$ and $\Psi = \left(\gamma\sigma_t^\alpha/|D|\right)^{1/2}\psi$. Here, we assume anomalous dispersion, such that $\mathrm{sgn}(D) = -1$.

We consider an ensemble of statistically stationary waves at $z = 0$ that obey the periodic boundary conditions. Each ensemble realization of the source field can then be expressed via a Fourier series of period T as

$$\Psi(t,0) = \sum_{n=-\infty}^{\infty} c_n e^{i2\pi nt/T}. \tag{4}$$

Here $\{c_n\}$ is a set of complex uncorrelated random amplitudes such that

$$\langle c_m^* c_n\rangle = \lambda_n\delta_{mn}, \tag{5}$$

where the angle brackets denote an ensemble average. We assume that the random phases of $\{c_n\}$ are uniformly distributed in the interval $(-\pi,\pi)$. Further, we choose the distribution of the mode weights $\{\lambda_n\}$ to be Gaussian

$$\lambda_n = \lambda_0 e^{-\zeta_c n^2}. \tag{6}$$

Here, ζ_c is a coherence parameter of the source ensemble; $\zeta_c \to \infty$ corresponds to a completely coherent source field with only the lowest-order mode $n = 0$ present, whereas $\zeta_c \to 0$ yields a nearly incoherent source field composed of a multitude of Fourier modes with almost identical coefficients.

The random phase model of the source, defined by Eqs. (4) and (5), is frequently employed to study classical or wave turbulence [7,26] and random wave revivals [27].

3. Results & discussion

We carried out numerical simulations of the FOT induced by the statistically stationary wave ensemble of Eq. (4) with the statistics given by Eqs. (5) and (6), by solving the FNLSE with a standard split-step Fourier technique. In the simulations, we introduced a numerical time window of size $T = 257.36$ with $N_t = 2^{12}$ temporal grid points. The propagation distance extends to $z = 10$ and discretized using $N_z = 2^{12}$ points. Furthermore, the source ensemble is completely characterized by the coherence parameter ζ_c; in our simulations, we chose $\zeta_c = 6.25$.

In Fig. 1, we display the evolution of the (dimensionless) intensity of a typical ensemble realization as a function of the (dimensionless) propagation distance z for a variable Lévy index. In Fig. 1(a), we display the case $\alpha = 1$. We can infer from

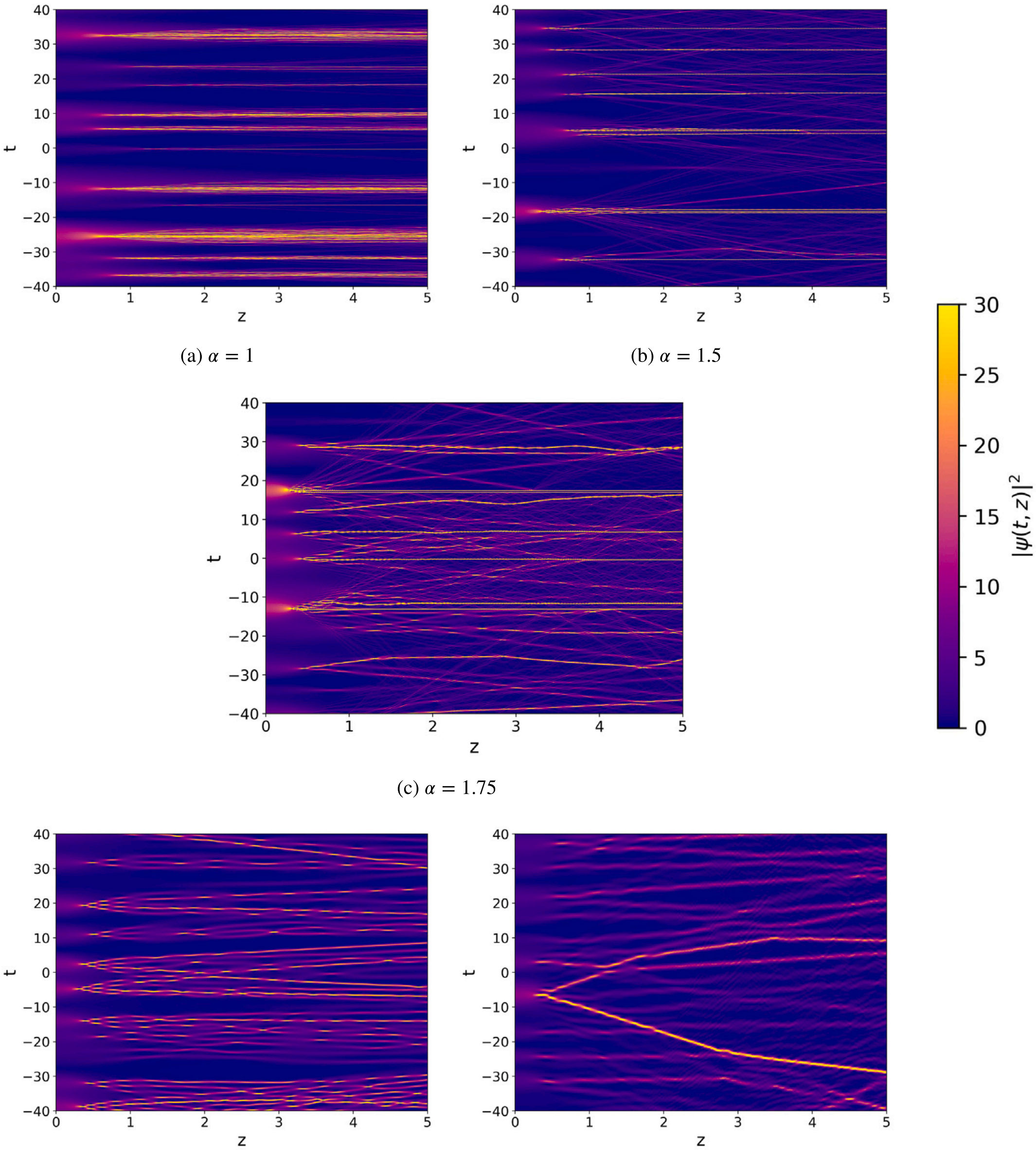

(a) $\alpha = 1$ (b) $\alpha = 1.5$

(c) $\alpha = 1.75$

(d) $\alpha = 2$ (e) $\alpha = 3$

Fig. 1. Intensity $|\Psi(t,z)|^2$ of an individual ensemble realization for a variable Lévy index α. All panels share the same color map shown on the right. (For interpretation of the references to color in this figure legend, the reader is referred to the web version of this article.)

the panel that the input random wave quickly gives rise to a set of random soliton-like structures surrounded by radiation waves. The latter arise due to the non-integrability of the FNLSE. Notice that random solitons persist over the propagation distance.

As we increase α to 1.5, we observe that radiation waves carry away less power, but random soliton trajectories start intersecting, indicating collisions (Fig. 1(b)). The system thus evolves into an interacting gas of random solitons. The soliton gas density and the frequency of soliton collisions increase markedly for $\alpha = 1.75$, as we can infer from Fig. 1(c). On comparing Figs. 1(c), (d), and (e), we can conclude that for $\alpha > 1.75$ not only the soliton gas density, but also the frequency of soliton collisions decreases with α. However, we note that Fig. 1(d) corresponds to the integrable NLSE case ($\alpha = 2$). This explains the regular nature of soliton collisions, resulting in a relatively uniform distribution of random solitons within the soliton gas volume. Our results for $\alpha = 2$ agree with previously reported results [7].

We stress that our extensive numerical simulations lead to two main conclusions. First, as the value of α approaches either end of the interval $\alpha \in (1,2)$, the random soliton collision frequency decreases. Second, soliton collisions become rare for $\alpha > 2$. The takeaway here is that FOT is strongly affected by the value of the Lévy index, and the collisions of individual solitons within a volume of random soliton gas appear to be *non-monotonically* affected by α in the range $\alpha \in (1, 2)$. To investigate the implications of these observations for the FOT statistics, we evaluated the probability density function (PDF) of normalized field intensities of the random field ensemble across varying propagation distances.

To find the normalized field intensity PDF, we formed an ensemble of $N = 10^3$ realizations, propagated each individual realization by the FNLSE and averaged over the ensemble. We present our results in Fig. 2 on a log-normal scale. We can infer from the figure that all panels share two common features. First, the black curve in each panel corresponds to the PDF at the source ($z = 0$). The PDF at $z = 0$ is very close, up to averaging errors, to a straight line corresponding to the exponential PDF of the field intensity of

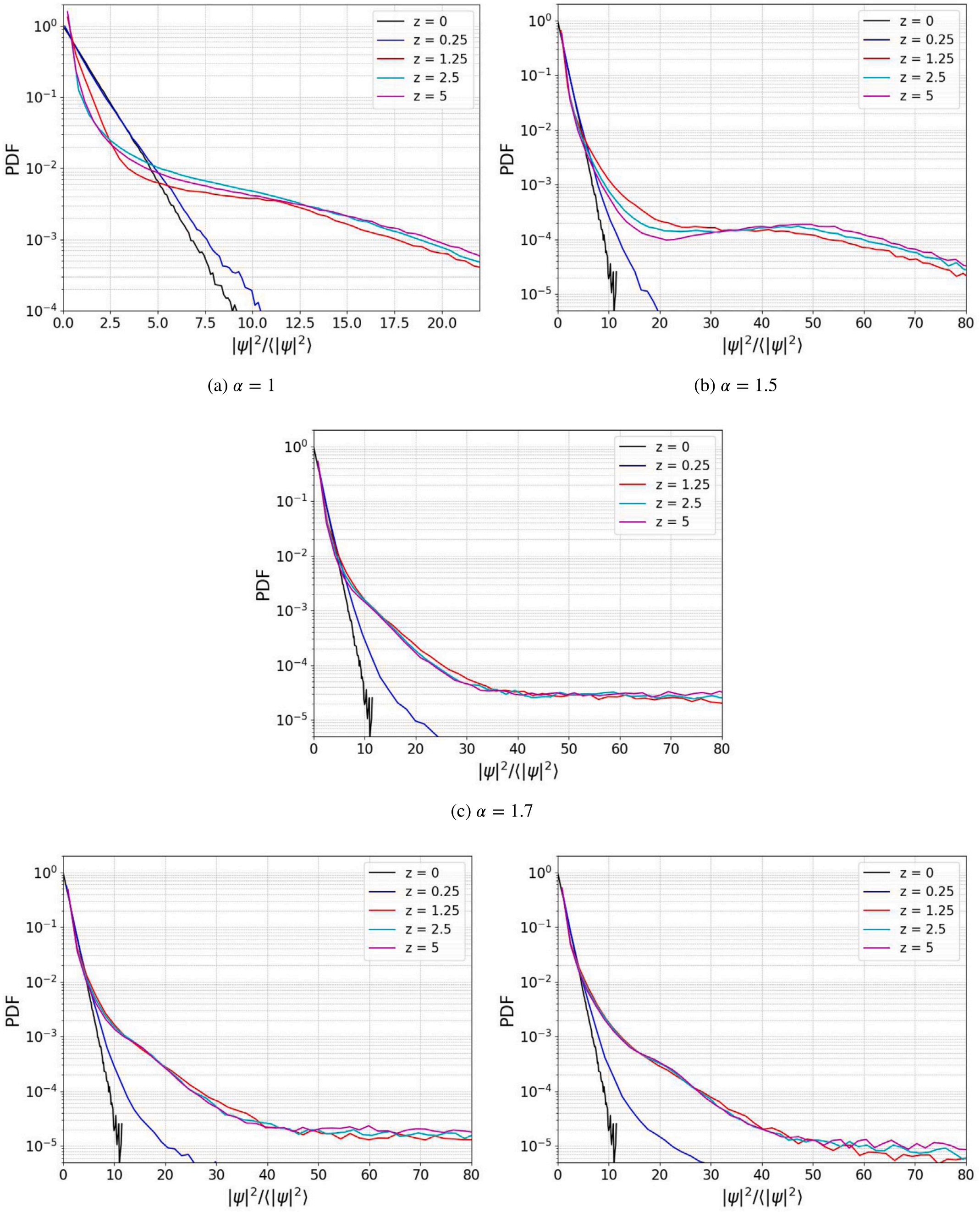

(a) $\alpha = 1$ (b) $\alpha = 1.5$ (c) $\alpha = 1.7$ (d) $\alpha = 1.75$ (e) $\alpha = 1.8$

Fig. 2. Probability density function (PDF) of the normalized field intensity for various Lèvy indices α in the range $1 \le \alpha \le 2$. Each panel shows PDFs for several propagation distances z, as is indicated in the corresponding legend.

our ensemble, which is an unmistakable signature of the Gaussian statistics of the source [28]. Second, we observe that the PDF in each panel quickly attains a stationary state, past which point no noticeable change occurs over further propagation. We carried out our simulations up to distance $z = 10$, but did not observe any discernible variation in the shape of the PDF or its tail structure beyond $z = 5$. Therefore, we omit any results corresponding to $z > 5$.

In Fig. 2(a), we show the PDF of the normalized field intensity over a variable propagation distance z for the low Lévy index case, $\alpha = 1$. We can infer from the panel by comparing the PDF at any $z \neq 0$ with the source PDF that as the propagating field triggers FOT in the medium, the statistics of the field transition from sub-Gaussian (thin-tailed) for low field intensities to super-Gaussian (fat-tailed) for high field intensities. We conjecture that in the low Lévy index FOT, fractional dispersion dominates for low-intensity ensemble realizations, while nonlinearity dominates for high-intensity realizations, resulting in mixed statistics of the field intensity.

However, as we increase the Lévy index beyond unity, the thin-tailed region of the PDF gradually diminishes in size and the PDF tail becomes progressively longer with α. This trend is clearly visible by comparing panels Fig. 2(b) through 2(e). In particular, the heavy-tailed nature of the PDF is especially vivid in panels Fig. 2(c), 2(d), and 2(e). We hypothesize that in the range of Lévy indices $1.7 \leq \alpha \leq 1.8$, FOT is primarily driven by the nonlinearity of the medium, leading to pronounced non-Gaussian statistics of the field intensity.

Our extensive simulations also indicate that for $\alpha > 1.8$, the heavy-tailed nature of the PDF gradually recedes with α. Thus, our statistical results correlate well with our simulations of the dynamics of individual ensemble realizations. Both sets of results point to the non-monotonic dependence of the FOT characteristics on the Lévy index in the interval $1.7 \leq \alpha \leq 1.8$.

We note that we performed an ensemble-size convergence test to check the validity of our choice of the number of realizations N. Fig. 3 shows the L^1 error (integrated absolute error) as a function of number of realizations for up to 10^4. We evaluated the L^1 error function with the PDF of $N = 10^3$ realizations taken as a reference. The figure clearly shows that the error decreases and stabilizes in the sense that we do not observe significant error fluctuations, within which the ensemble size used in our simulations lies. The figure indeed shows an example of these results; however, we stress that the results obtained for all other Lévy indices are similar.

Moreover, since the Riesz derivative in Eq. (2) is implemented in Fourier space through $|\omega|^\alpha$, possible high-frequency effects require careful consideration. For this reason, we performed targeted numerical tests, including possible effects associated with spectral truncation and the finite size of the temporal window, to ensure that our numerical results are not strongly influenced by undesired computational effects.

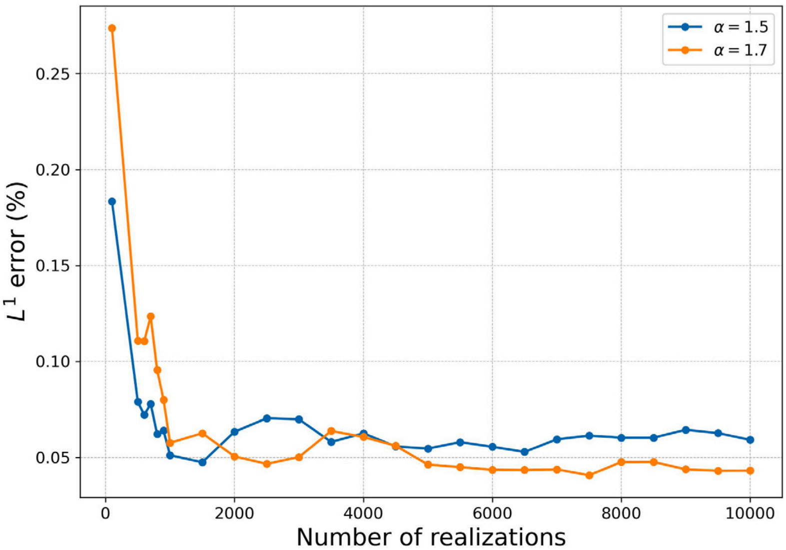

Fig. 3. Ensemble-size convergence test presenting the L^1 error (integrated absolute error) as a function of the number of realizations for up to 10^4. Displayed examples are for $\alpha = 1.5$ and $\alpha = 1.7$.

In addition, to make our qualitative conclusions about the heavy tails of the PDF more quantitative, we computed the tail exponent as a function of the Lévy index α as shown in Fig. 4. We inferred the value of the exponent from a power-law fit to the PDF tail for normalized intensities satisfying $I > I_0$ where I_0 is chosen to satisfy the rogue wave threshold condition [29]. The figure clearly demonstrates that the parameter range $1.7 \leq \alpha \leq 1.8$ corresponds to the lowest tail exponent values, which supports our qualitative conclusions from Fig. 2.

To highlight the scale of deviations of FOT from Gaussian statistics in the parameter range $1.7 \leq \alpha \leq 1.8$, we fit the PDF of the normalized intensity at $z = 5$ for the FOT with $\alpha = 1.75$ with a Lomax distribution. In Fig. 5, we show the Lomax fit of the PDF. The Lomax distribution is a heavy-tailed Pareto type-II probability distribution frequently encountered in multidisciplinary field contexts in economics [30], engineering [31], and optics [32]. The Lomax PDF is defined as [33,34]:

$$p_{\mathrm{L}}(x) = \frac{\beta}{s}\left(1 + \frac{x}{s}\right)^{-(\beta+1)}, \tag{7}$$

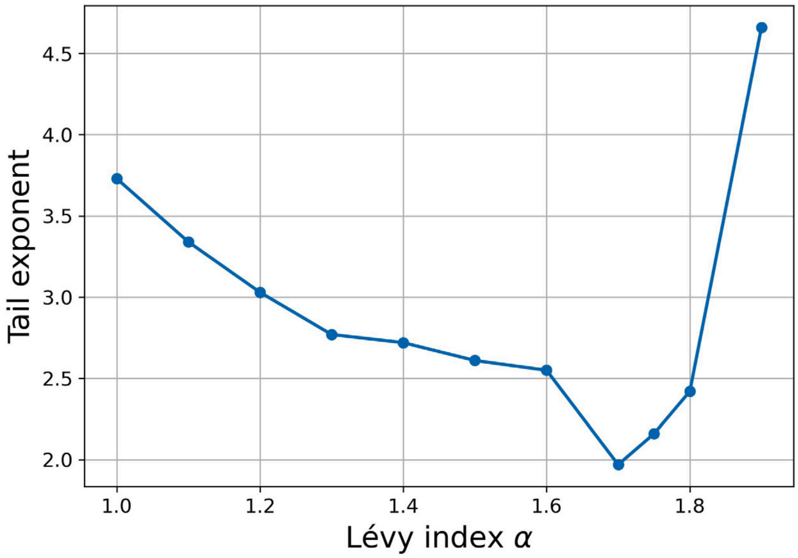

Fig. 4. Tail exponent as a function of the Lévy index α for values in the range $1 \leq \alpha \leq 2$.

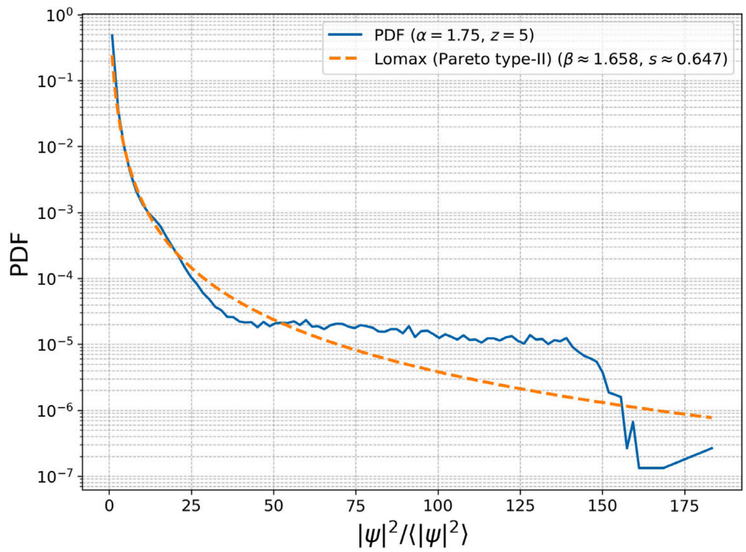

Fig. 5. MLE Lomax of the PDF of the normalized field intensity of the FOT with $\alpha = 1.75$ in the stationary regime at $z = 5$.

where β and s are the shape and scale parameters, respectively. The maximum likelihood estimation (MLE) yields the values: $\beta \approx 1.658$ and $s \approx 0.647$. The fit clearly emphasizes the heavy-tailed nature of the PDF. Although $\beta < 2$, it should only be interpreted as an indication that the corresponding ideal Lomax distribution is, in fact, a divergent one, underscoring the extreme heavy-tailed nature of the intensity statistics for $\alpha = 1.75$. We stress that the selection of the Lomax distribution as a fit here was merely to illustrate the departure from Gaussian statistics.

So far, we have explored the global deviation of FOT statistics from Gaussian. We now examine whether deviations from Gaussianity become more pronounced at fine scales of FOT. To this end, we consider the real part of the field, $S(t) = \Re(\Psi(t, \tilde{z}))$ where $\tilde{z}$ indicates that the propagation distance corresponds to the stationary regime. We can then define a high-pass filtered function $S_{\xi}^{>}(t)$ as:

$$S_{\xi}^{>}(t) = \int_{|\omega|>\xi} d\omega\, e^{i\omega t}\, \tilde{S}(\omega), \tag{8}$$

where ξ is a cut-off frequency of the filter. Next, we define a high-pass kurtosis κ by the expression:

$$\kappa(\xi) = \frac{\langle (S_{\xi}^{>}(t))^4 \rangle}{\langle (S_{\xi}^{>}(t))^2 \rangle^2}. \tag{9}$$

The monotonic increase of κ with the filter frequency establishes a test for the intermittency of the system [1]. To verify whether FOT is intermittent, we evaluated the kurtosis as a function of ξ for various Lévy indices. We stress that we evaluated $\kappa(\xi)$ at $z = 5$, where the statistics have reached a steady state.

In Fig. 6, we show the filtered kurtosis as a function of ξ for the Lévy index α in the interval $1 \leq \alpha \leq 2$ along with the corresponding 95% bootstrap confidence interval for each trace. A kurtosis greater than 3 indicates a heavy-tailed probability distribution [28,35]. Fig. 6(a) reports the kurtosis values that correspond to the coherence parameter $\zeta_c = 6.25$, used throughout the preceding analysis. We can see in the figure that the kurtosis monotonically increases with ξ for any α, implying the FOT intermittency. However, the kurtosis growth with the cut-off frequency is especially pronounced in the range $1.7 \leq \alpha \leq 1.8$. Furthermore, to demonstrate that the observed behavior is not specific to a particular coherence state of the source, we present the kurtosis values for $\zeta_c = 10$ in Fig. 6(b). The figure clearly evidences FOT intermittency and its non-monotonic dependence on the Lévy index. This is aligned with our previous results, indicating that the interval $1.7 \leq \alpha \leq 1.8$ plays a special role in generating extreme events and triggering highly non-Gaussian FOT with intense, sporadic local turbulent bursts.

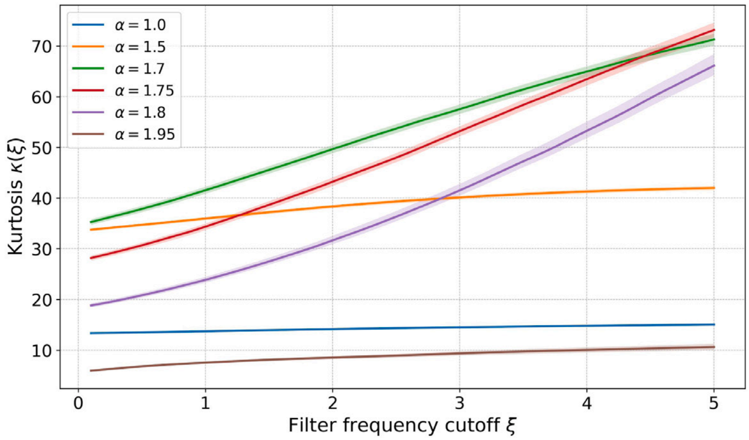

(a) $\zeta_c = 6.25$

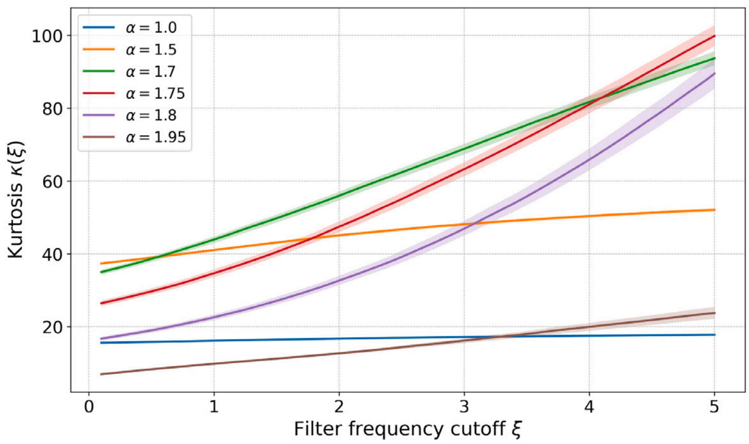

(b) $\zeta_c = 10$

Fig. 6. Kurtosis of the high-pass filtered real part of the field as a function of the cut-off frequency of the filter for (a) $\zeta_c = 6.25$ and (b) $\zeta_c = 10$, evaluated in the stationary regime at $z = 5$ for various Lévy indices in the range $1 \leq \alpha \leq 2$ with shaded bands illustrating 95% bootstrap confidence intervals.

4. Conclusions

We have introduced the concept of fractional wave turbulence and systematically studied its statistical properties. We have shown that the probability density function of normalized field intensities generated by a statistically stationary source and propagating in a nonlinear optical medium with fractional dispersion is strongly non-Gaussian and the deviation from Gaussian statistics non-monotonically depends on the Lévy index of the system. We have also revealed the intermittency of the fractional optical turbulence and demonstrated its non-monotonic dependence on the Lévy index. We have identified an interval of Lévy indices, $1.7 \leq \alpha \leq 1.8$, where both the non-Gaussianity and the FOT intermittency are particularly strong. Instructively, a complementary study of non-stationary soliton turbulence governed by the FNLSE indicated the increased probability of rogue wave formation at $\alpha = 1.8$ [25]. Thus, we have unveiled a parameter region in which both global and local statistics of the system are most affected by the turbulence.

Finally, it has come to our attention that the FNLSE model of FOT is mathematically equivalent to a previously introduced model nonlinear equation to describe weak dispersive wave turbulence [36]. However, we stress that our results are obtained in the strong turbulence regime that is complementary to weak wave turbulence explored in [36–38]. Within the framework of weak dispersive wave turbulence, linear dispersion dominates nonlinearity which, together with a random phase approximation, implies Gaussian, or nearly Gaussian statistics of the wave system. As a result, the system evolution can be described within a closed kinetic equation for the second-order field correlations. On the contrary, in the strong turbulence regime that we study, characteristic nonlinear and dispersion lengths are of the same order, leading to a subtle interplay of linear and nonlinear effects. The latter opens the door to highly non-Gaussian statistics of random waves, extreme events emerging in long heavy tails of the probability distribution of wave powers, and pronounced intermittency with non-monotonic dependence on the Lévy index of FOT. Although we do not have a definitive explanation of the non-monotonic nature of FOT statistics at the moment, we believe that the discovered parameter region warrants further investigation and our findings can inform future research into fractional optical turbulence.

CRediT authorship contribution statement

Saad Alhadlaq: Writing – review & editing, Writing – original draft, Software, Formal analysis. **Sergey A. Ponomarenko:** Writing – review & editing, Writing – original draft, Supervision, Funding acquisition, Conceptualization.

Declaration of competing interest

The authors declare that they have no known competing financial interests or personal relationships that could have appeared to influence the work reported in this paper.

Acknowledgments

The authors acknowledge support from the Natural Sciences and Engineering Research Council of Canada (NSERC) (RGPIN-2025-04064).

Data availability

No data was used for the research described in the article.

References

[1] Frisch U, Donnelly RJ. Turbulence: The legacy of A.N. Kolmogorov. American Institute of Physics; 1996.
[2] Liu L, Hu F. Finescale clusterization intermittency of turbulence in the atmospheric boundary layer. J Atmos Sci 2020;77(7):2375–92.
[3] Zheng Y, Liu H, Chamorro LP, Zhao Z, Li Y, Zheng Y, Tang K. Impact of turbulence level on intermittent-like events in the wake of a model wind turbine. Renew Energy 2023;203:45–55.
[4] Kraichnan RH. Intermittency in the very small scales of turbulence. Phys Fluids 1967;10(9):2080–2.
[5] Frisch U, Morf R. Intermittency in nonlinear dynamics and singularities at complex times. Phys Rev A 1981;23(5):2673.
[6] Li Y, Meneveau C. Origin of non-Gaussian statistics in hydrodynamic turbulence. Phys Rev Lett 2021;95:164502.
[7] Randoux S, Suret P. Integrable turbulence with nonlinear random optical waves. In: Rogue and shock waves in nonlinear dispersive media. Springer; 2016, p. 277–307.
[8] Zakharov VE. Turbulence in integrable systems. Stud Appl Math 2009;122(3):219–34.
[9] Pelinovsky EN, Shurgalina EG, Sergeeva AV, Talipova TG, El GA, Grimshaw RHJ. Two-soliton interaction as an elementary act of soliton turbulence in integrable systems. Phys Lett A 2013;377(3–4):272–5.
[10] Agafontsev DS, Zakharov VE. Integrable turbulence and formation of rogue waves. Nonlinearity 2015;28(8):2791–821.
[11] Kivshar YS, Agrawal GP. Optical solitons: from fibers to photonic crystals. Academic Press; 2003.
[12] Walczak P, Randoux S, Suret P. Optical rogue waves in integrable turbulence. Phys Rev Lett 2015;114(14):143903.
[13] Laskin N. Fractional quantum mechanics and Lévy path integrals. Phys Lett A 2000;268(4–6):298–305.
[14] Longhi S. Fractional Schrödinger equation in optics. Opt Lett 2015;40:1117.
[15] Malomed BA. Optical solitons and vortices in fractional media: a mini-review of recent results. Photonics 2021;8(9):353.
[16] Secchi S, Squassina M. Soliton dynamics for fractional Schrödinger equations. Appl Anal 2014;93:1702.
[17] Klein C, Sparber C, Markowich P. Numerical study of fractional nonlinear Schrödinger equations. Proc R Soc A: Math Phys Eng Sci 2014;470(2172).
[18] Zeng L, Zeng J. One-dimensional solitons in fractional Schrödinger equation with a spatially periodical modulated nonlinearity: nonlinear lattice. Opt Lett 2019;44:2661.
[19] Qiu Y, Malomed BA, Mihalache D, Zhu X, Peng X, He Y. Stabilization of single-and multi-peak solitons in the fractional nonlinear Schrödinger equation with a trapping potential. Chaos Solitons Fractals 2020;140:110222.
[20] Duo S, Lakoba TI, Zhang Y. Dynamics of plane waves in the fractional nonlinear Schrödinger equation with long-range dispersion. Symmetry 2021;13:1394.
[21] Liang R, Wang Y. Gibbs dynamics for fractional nonlinear Schrödinger equations with weak dispersion. Comm Math Phys 2024;405(10):250.
[22] Malomed BA. Basic fractional nonlinear-wave models and solitons. Chaos: Interdiscip J Nonlinear Sci 2024;34(2).
[23] Liu S, Zhang Y, Malomed BA, Karimi E. Experimental realisations of the fractional Schrödinger equation in the temporal domain. Nat Commun 2023;14(1):222.

[24] Liu S, Zhang Y, Virally S, Karimi E, Malomed BA, Seletskiy DV. Experimental emulator of pulse dynamics in fractional nonlinear Schrödinger equation. Laser Photonics Rev 2025;19(8):2401714.
[25] Zhong M, Weng W, Guo B, Yang Z. The fractional nonlinear Schrödinger equation: Soliton turbulence, modulation instability, and extreme rogue waves. Chaos 2025;35:013131.
[26] Dudley JM, Genty G, Mussot A, Chabchoub A, Dias F. Rogue waves and analogies in optics and oceanography. Nat Rev Phys 2019;1(11):675–89.
[27] Bai Y, Cai Y, Liang C, Ponomarenko SA. Regular and irregular revivals of quasi-periodic random waves. 2026, arXiv preprint arXiv:2603.16371.
[28] Papoulis A. Random variables and stochastic processes. McGraw Hill; 1991.
[29] Dudley JM, Dias F, Erkintalo M, Genty G. Instabilities, breathers and rogue waves in optics. Nat Photonics 2014;8:755.
[30] Corbellini A, Crosato L, Ganugi P, Mazzoli M. Fitting Pareto II distributions on firm size: Statistical methodology and economic puzzles. In: Advances in data analysis: Theory and applications to reliability and inference, data mining, bioinformatics, lifetime data and neural networks. Springer; 2009, p. 321–8.
[31] Ijaz M. Bayesian estimation of the shape parameter of lomax distribution under uniform and jeffery prior with engineering applications. Gazi Univ J Sci 2021;34(2):562–77.
[32] Ge GR, Rolland JP, Parker KJ. Speckle statistics of biological tissues in optical coherence tomography. Biomed Opt Express 2021;12(7):4179–91.
[33] Giles DE, Feng H, Godwin RT. On the bias of the maximum likelihood estimator for the two-parameter lomax distribution. Comm Statist Theory Methods 2013;42(11):1934–50.
[34] Arnold BC. Pareto and generalized Pareto distributions. In: Modeling income distributions and Lorenz curves. Springer; 2008, p. 119–45.
[35] Onorato M, Osborne AR, Serio M, Cavaleri L. Modulational instability and non-Gaussian statistics in experimental random water-wave trains. Phys Fluids 2005;17(7).
[36] Majda AJ, McLaughlin DW, Tabak EG. A one-dimensional model for dispersive wave turbulence. J Nonlinear Sci 1997;6:9–44.
[37] Cai D, Majda AJ, McLaughlin DW, Tabak EG. Spectral bifurcations in dispersive wave turbulence. PNAS 1999;96:14216–21.
[38] Cai D, Majda AJ, McLaughlin DW, Tabak EG. Dispersive wave turbulence in one dimension. Phys D 2001;152:551–72.